Supplementary Information (SI) for Journal of Materials Chemistry A.

Dual Substitution in Cationic and Anionic Sublattices of Lithium Indium Chloride for High-Performance Solid-State Lithium Metal Batteries

Farzaneh Bahmani [a]*, and Alevtina White Smirnova [a, b,] *

[a] Materials Engineering and Science program, South Dakota Mines, South Dakota 57701, USA

[b] Department of Chemistry, Biology, and Health Sciences, South Dakota Mines, South Dakota 57701, USA

Farzaneh Bahmani, Email: farzaneh.bahmani@mines.sdsmt.edu.

Corresponding author: Dr. Alevtina White Smirnova, Email: Alevtina.Smirnova@sdsmt.edu.

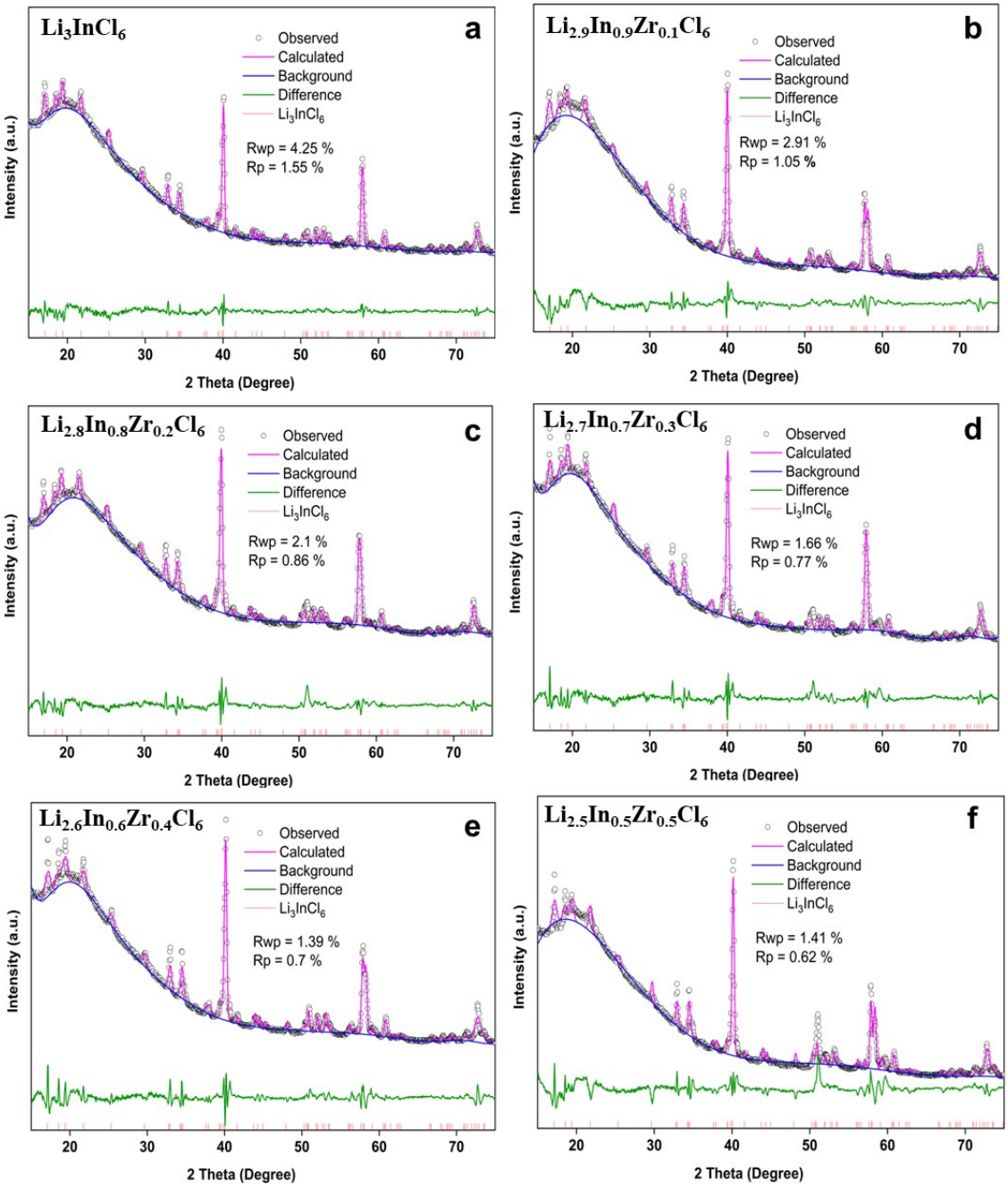

Fig. S1 Rietveld-refinements of $Li_{3-x}In_{1-x}Zr_xCl_6$ ($0 \leq x < 0.6$) electrolytes from XRD data.

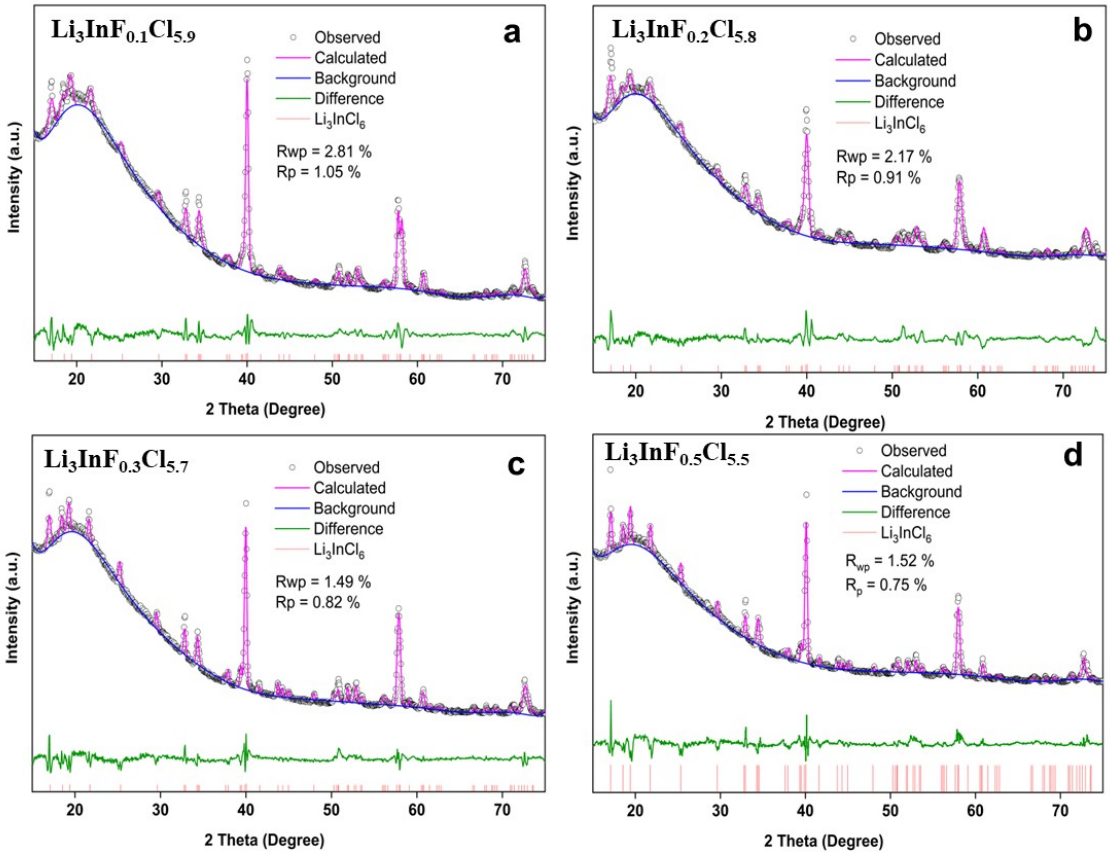

Fig. S2 Rietveld-refinements of $Li_3InCl_{6-y}F_y$ (0 <y <0.6) electrolytes from XRD data.

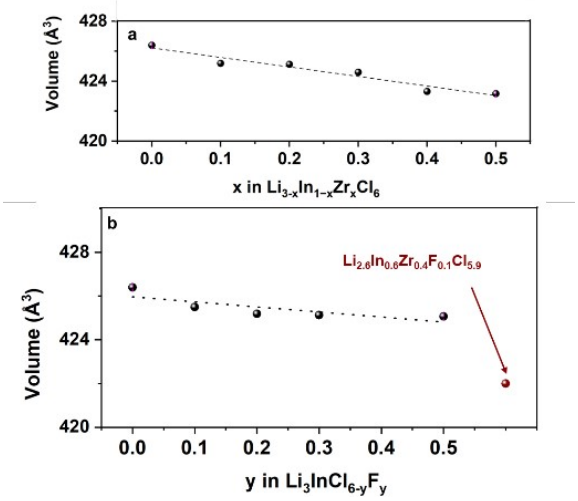

Fig. S3 Unit cell size for $Li_{3-x}In_{1-x}Zr_xCl_6$ ($0 \le x < 0.6$), $Li_3InF_yCl_{6-y}$ ($0 \le y < 0.6$) and $Li_{2.6}In_{0.6}Zr_{0.4}F_{0.1}Cl_{5.9}$ electrolytes.

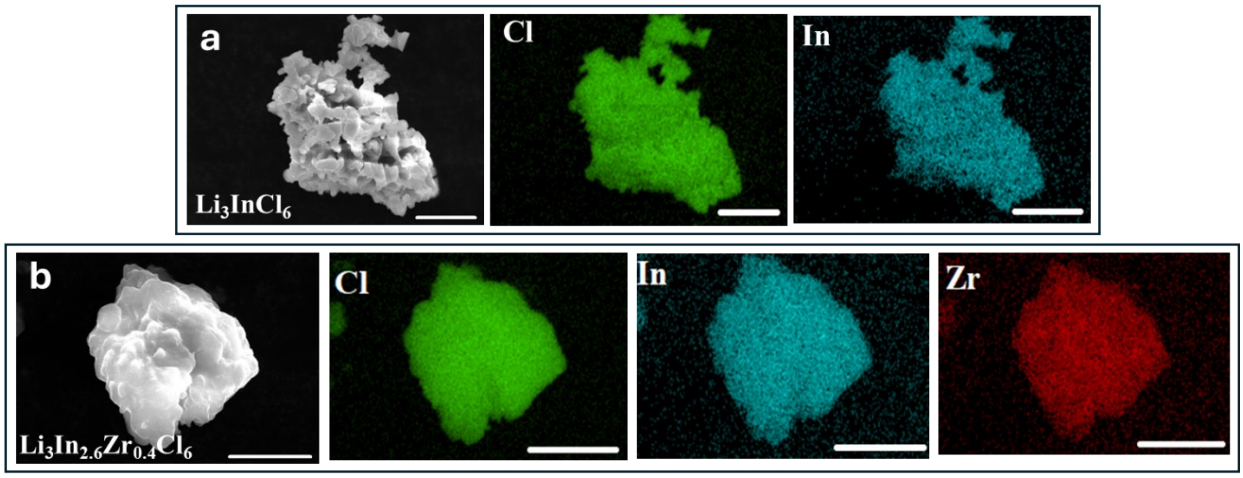

Fig. S4 The electron images with the corresponding EDS maps for Li_3InCl_6 and $Li_3In_{2.6}Zr_{0.4}Cl_6$ (scale bar: 10 μm).

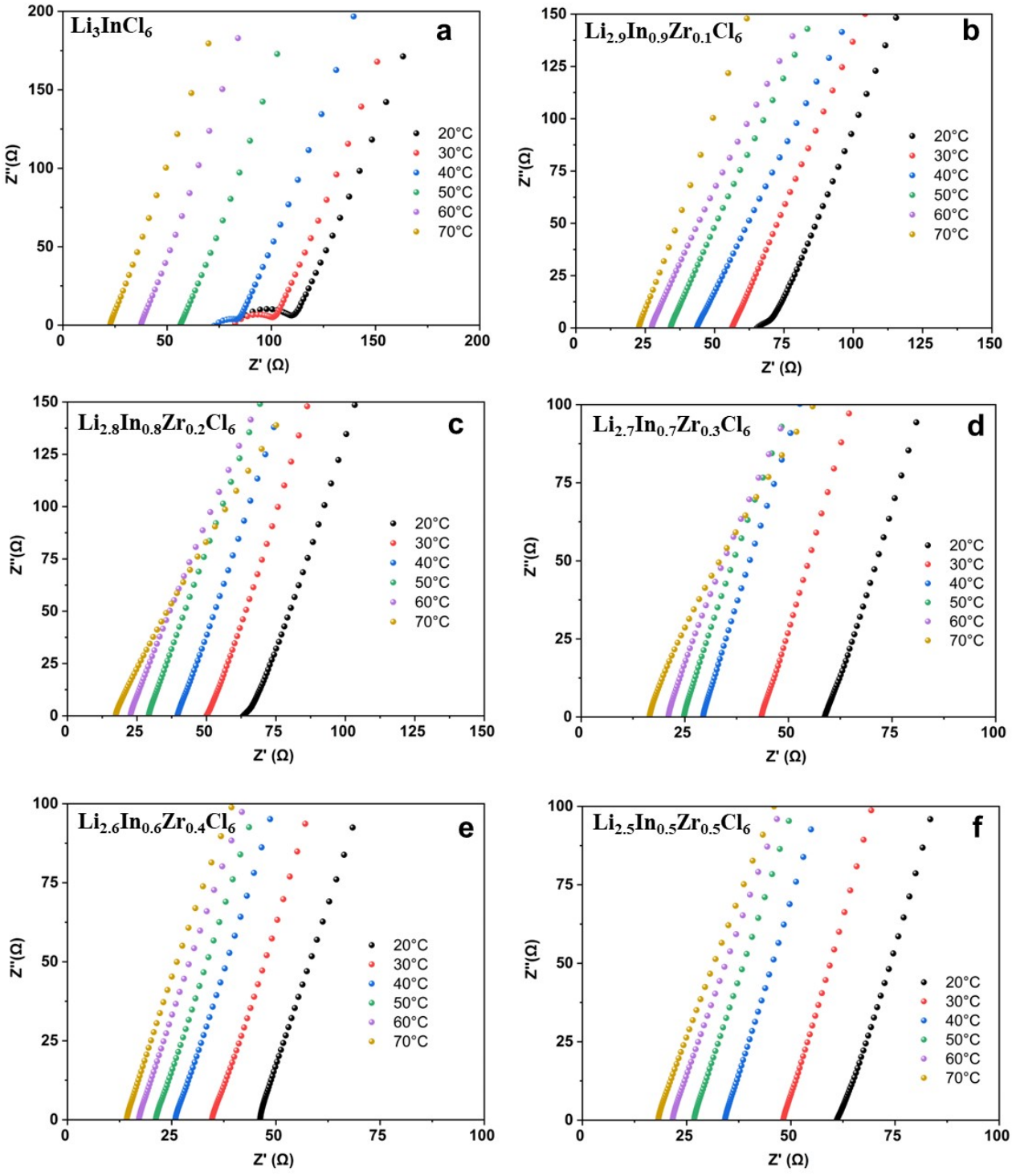

Fig. S5 EIS spectra of $Li_{3-x}In_{1-x}Zr_xCl_6$ ($0 \le x < 0.6$) electrolytes at different temperatures.

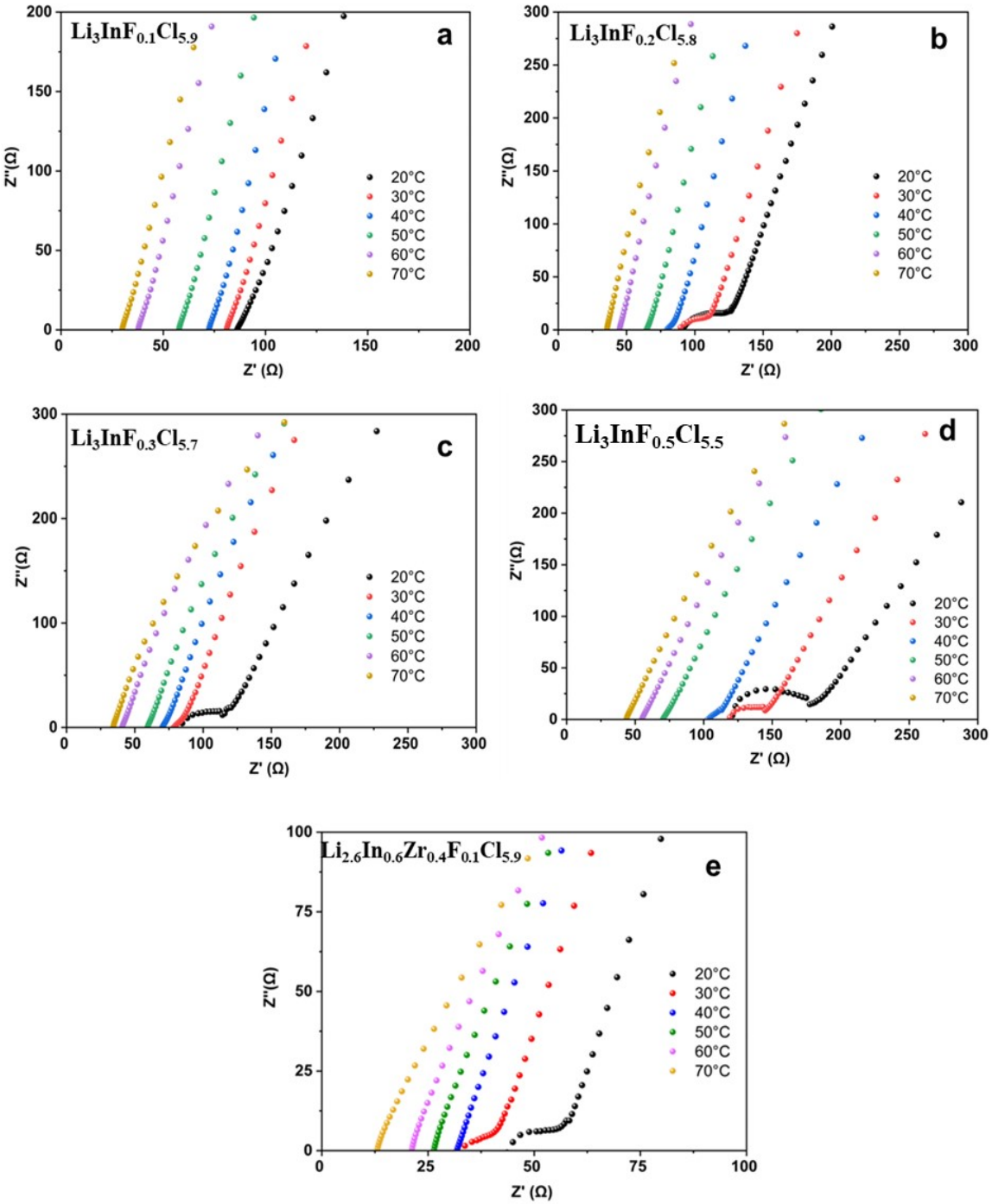

Fig. S6 EIS spectra of $Li_3InF_yCl_{6-y}$ ($0 \le y < 0.6$) and $Li_{2.6}In_{0.6}Zr_{0.4}F_{0.1}Cl_{5.9}$ electrolytes at different temperatures.

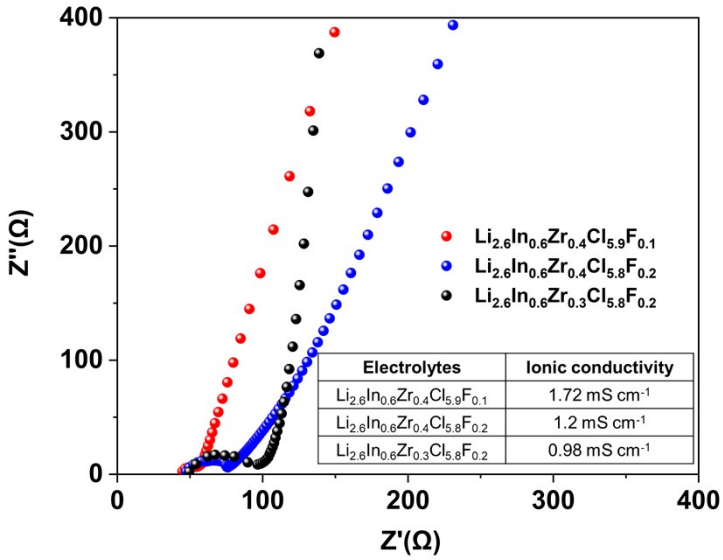

Fig S7. EIS plots of co-doped Li_3InCl_6 with different ratios of Zr and F at 20 °C

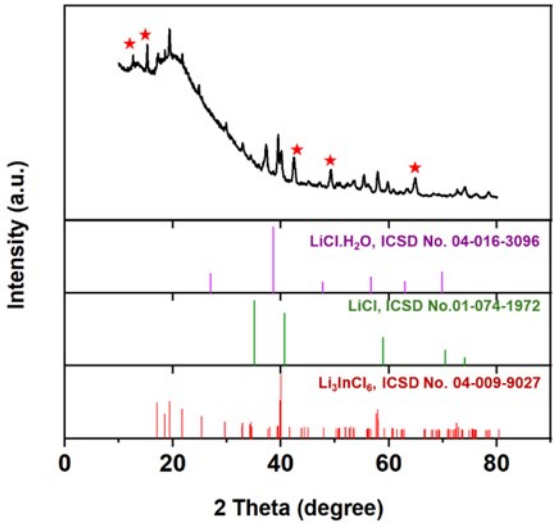

Fig. S8 Comparison of the XRD patterns of Li_3InCl_6 electrolyte after 5 h exposure to air with 14% humidity with XRD pattern of LiCl, $LiCl.H_2O$.

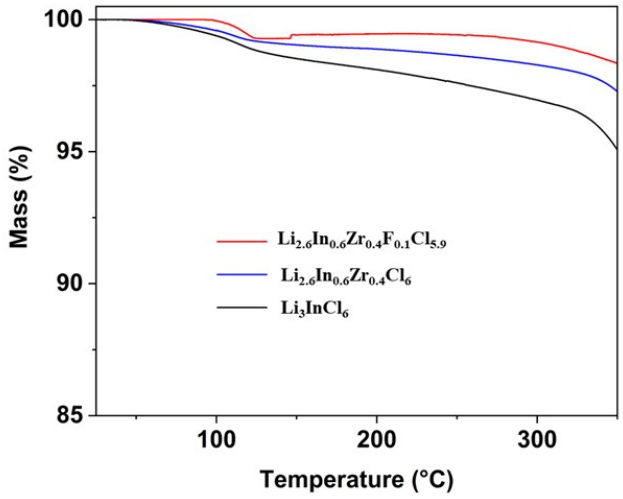

Fig S9. Thermogravimetry (TG) analysis of Li_3InCl_6, $Li_{2.6}In_{0.6}Zr_{0.4}Cl_6$, and $Li_{2.6}In_{0.6}Zr_{0.4}F_{0.1}Cl_{5.9}$ electrolytes after 5 h of air exposure.

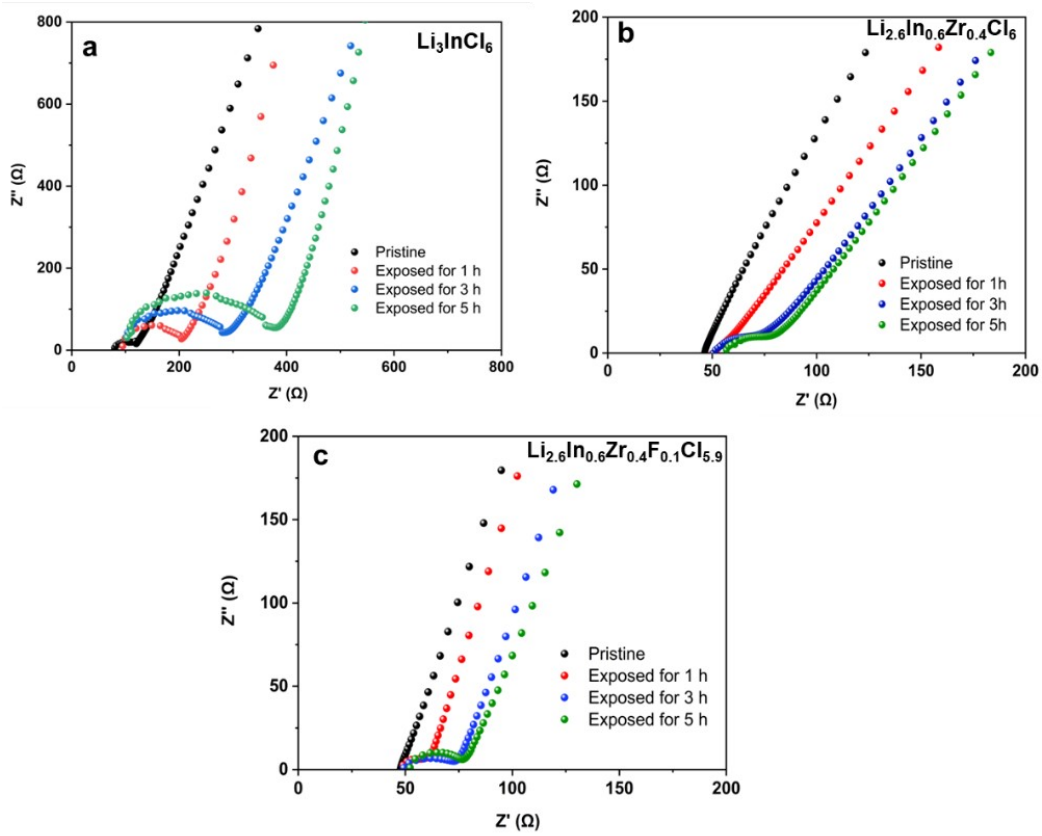

Fig. S10 EIS plots for Li_3InCl_6, $Li_{2.6}In_{0.6}Zr_{0.4}Cl_6$, and $Li_{2.6}In_{0.6}Zr_{0.4}F_{0.1}Cl_{5.9}$ electrolytes over time of exposure.

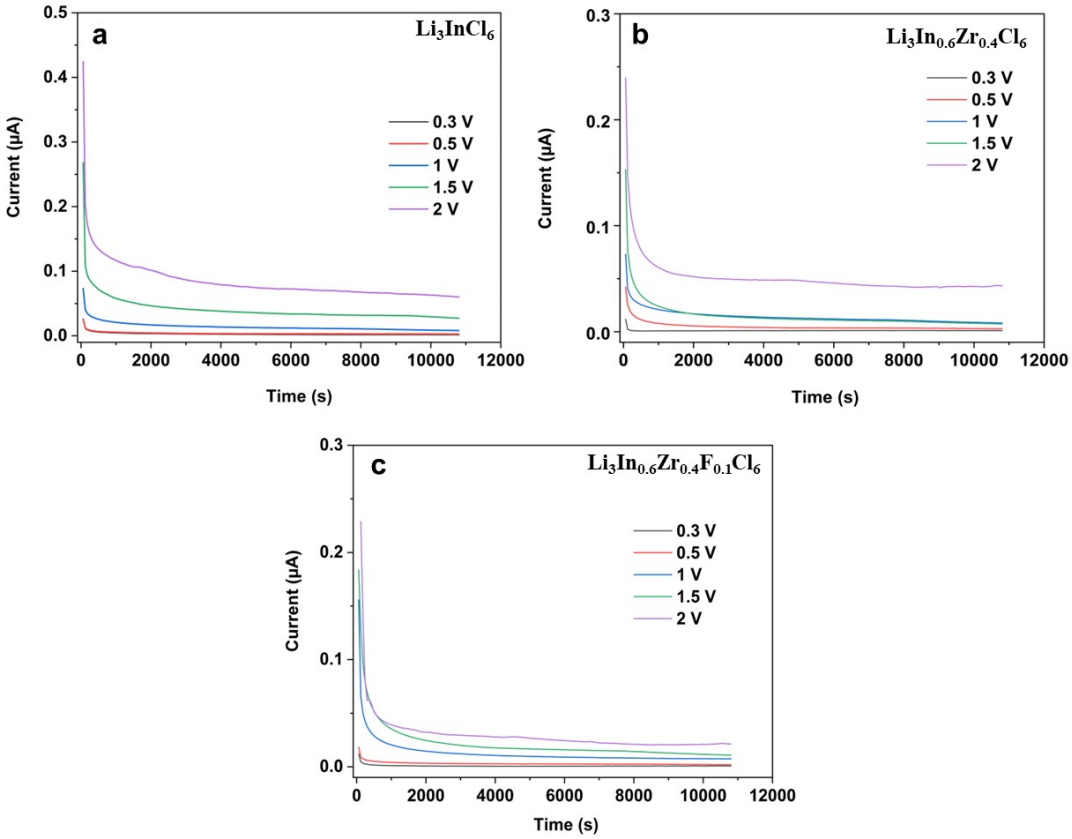

Fig. S11 Current–time curves of the SS|SSE|SS symmetric cells for Li_3InCl_6, $Li_{2.6}In_{0.6}Zr_{0.4}Cl_6$, and $Li_{2.6}In_{0.6}Zr_{0.4}F_{0.1}Cl_{5.9}$ electrolytes under different DC polarization.

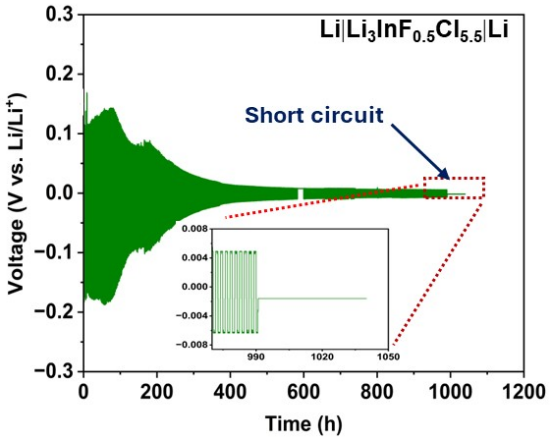

Fig. S12 The galvanostatic cycling data for Li|$Li_3InF_{0.5}Cl_{5.5}$|Li symmetric cells at a current density of 0.05 mA cm^{-2}.

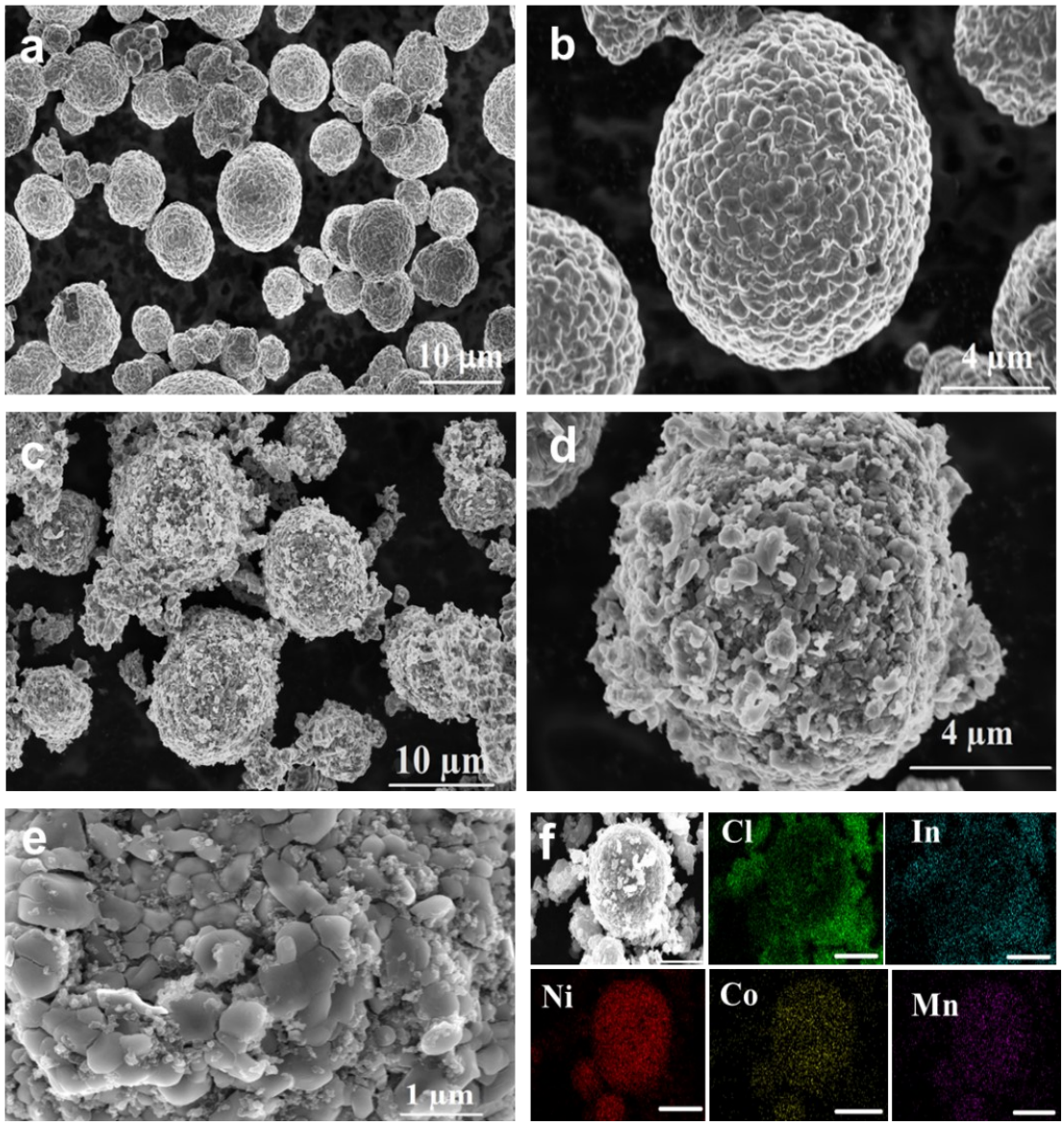

Fig. S13 (a, b) SEM images of NMC811 at different magnifications. (c, d) SEM images of cathode mixture (NMC811-Li_3InCl_6-CB) at different magnifications. (e, f) SEM and EDS X-ray maps of cathode mixture (scale bar: 5 µm).

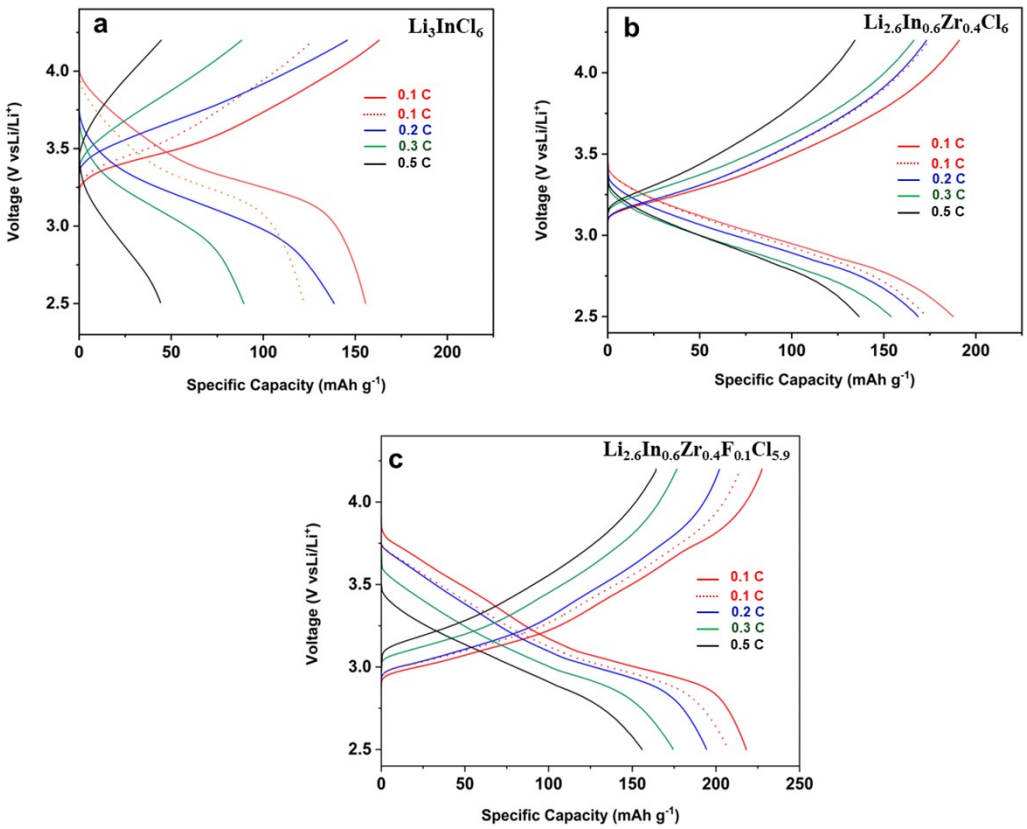

Fig. S14 Charge−discharge profile of NMC811-SSE-CB|SSE|LPSC|Li−In cells for Li_3InCl_6, $Li_{2.6}In_{0.6}Zr_{0.4}Cl_6$, and $Li_{2.6}In_{0.6}Zr_{0.4}F_{0.1}Cl_{5.9}$ electrolytes at different C-rates.

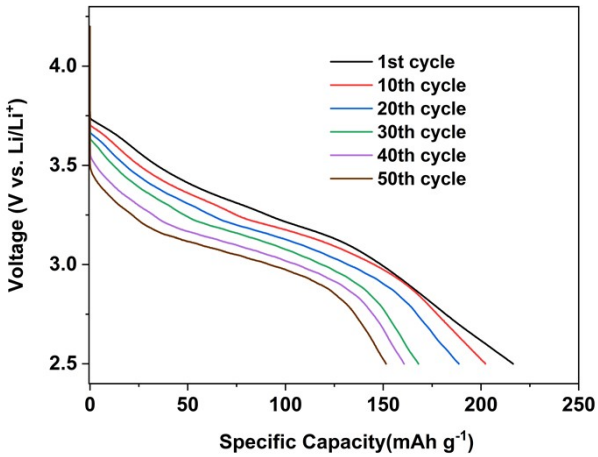

Fig. S15 Discharge profile of NMC8-SSE-CB|$Li_{2.6}In_{0.6}Zr_{0.4}F_{0.1}Cl_{5.9}$|LPSC|Li−In cell during cycling at 0.1 C.

Table S1. Structural data for Li_3InCl_6 obtained from Rietveld refinement.

Atom	Wyckoff	*x/a*	*y/b*	*z/c*	Occ
In	2a	0	0	0	0.889
In	4g	0	0.316	0	0.07
Li	4h	0	0.216	0.5	1
Li	2d	0.5	0	0.5	1
Cl	4i	0.2450	0	0.7568	1
Cl	8j	0.2421	0.1668	0.2362	1

Table S2. Structural data for $Li_{2.6}In_{0.6}Zr_{0.4}F_{0.1}Cl_{5.9}$ obtained from Rietveld refinement.

Atom	Wyckoff	*x/a*	*y/b*	*z/c*	Occ
In	2a	0	0	0	0.394
Zr	2a	0	0	0	0.282
In	4g	0	0.3373	0	0.12
Zr	4g	0	0.3373	0	0.07
Li	4h	0	0.226	0.5	0.82
Li	2d	0.5	0	0.5	0.74
Cl	4i	0.2397	0	0.7622	1
Cl	8j	0.2435	0.16914	0.2360	0.897
F	8j	0.2435	0.16914	0.2360	0.065

Table S3. Resistance of the NMC811-SSE-CB|SSE|LPSCl|Li−In for Li_3InCl_6, $Li_{2.6}In_{0.6}Zr_{0.4}Cl_6$, and $Li_{2.6}In_{0.6}Zr_{0.4}F_{0.1}Cl_{5.9}$ electrolytes after cycling fitted by the following equivalent electric circuit.

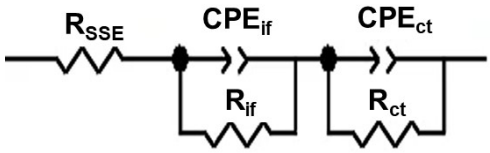

Electrolytes	R_{SSE} (Ω)	R_{if} (Ω)	R_{ct} (Ω)
Li_3InCl_6	105.1	491.7	1197.4
$Li_{2.6}In_{0.6}Zr_{0.4}Cl_6$	93.9	166.4	732.2
$Li_{2.6}In_{0.6}Zr_{0.4}F_{0.1}Cl_{5.9}$	86.4	64.58	537.9